# Assessment of radiometric correction methods for ADS40 imagery

LAURI MARKELIN, Finland; EIJA HONKAVAARA, Finland; DANIEL SCHLÄPFER, Switzerland; STÉPHANE BOVET, Switzerland; ILKKA KORPELA, Finland

**Keywords**: Reflectance, aerial images, radiometric correction, vicarious calibration

**Summary:** This article presents the results of an assessment of radiometric correction methods of images taken by the large-format aerial, photogrammetric, multispectral pushbroom camera Leica Geosystems ADS40. The investigation was carried out in the context of the multi-site EuroSDR project "Radiometric aspects of digital photogrammetric images". Images were collected at the forestry research test site Hyytiälä, Finland in August, 2008. Two processing workflows were evaluated: one based on the photogrammetric software Leica XPro, which in radiometric processes relies on physical modeling and information collected from the imagery only, and one based on ATCOR-4, which is software dedicated to physical atmospheric correction of airborne multi-, hyperspectral and thermal scanner data, and can be operated either with or without in-situ reflectance and atmospheric observations. Outputs of these processes are reflectance images. Three participants processed the data with several processing options which resulted in a total of 12 different radiometrically corrected reflectance images. The data analysis was based on field and laboratory reflectance measurements of reference reflectance targets and field measurements of permanent targets (asphalt, grass, gravel). Leica XPro provided up to 5 % reflectance accuracy without any ground reference and ATCOR-4 provided reflectance accuracy better than 5 % with vicarious in-flight radiometric calibration of the sensor. The results show that the radiometric correction of multispectral aerial images is possible in an efficient way in the photogrammetric production environment.

**Zusammenfassung:** Dieser Beitrag präsentiert die Ergebnisse einer Untersuchung von Methoden zur radiometrischen Korrektur von Aufnahmen der großformatigen photogrammetrischen Luftbild-Zeilenkamera Leica Geosystems ADS40. Die Untersuchung wurde im Rahmen EuroSDR Projekts "Radiometric aspects of digital photogrammetric images" durchgeführt. Im August 2008 wurden hiezu Bilder über dem forstwirtschaftlichen Testgebiet Hyytiälä in Finnland erfasst. Zwei Verfahren der Prozessierung wurden evaluiert. Das erste Verfahren baut auf der photogrammetrischen Software Leica XPro auf, welche sich in radiometrischen Prozessen auf physikalische Modelle bzw. Informationen verlässt, die ausschließlich aus den Bildern abgeleitet warden kann. Das zweite Verfahren baut auf ATCOR-4 auf, einem Software-Paket welches zur physikalischen atmosphärischen Korrektur flugzeuggestützter multi- und hyperspektraler Bilder sowie Bildern von Thermalscannern dient und sowohl mit als auch ohne in-situ Beobachtungen des Rückstreuverhaltens bzw. der atmosphärischen Bedingungen operieren kann. Das Ergebnis dieser Prozesse sind Bilder, welche den Reflexionsgrad darstellen. Drei Teilnehmer prozessieren die Daten mit verschiedenen Optionen, was insgesamt zu 12 verschiedenen radiometrisch korrigierten Bildern führte. Die Analyse der Daten basierte auf Messungen des Reflexionsgrads von Referenzsignalen im Feld und im Labor sowie auf Feldmessungen von permanenten Objekten (Asphalt, Gras, Schotter). Leica XPro lieferte eine Genauigkeit des Reflexionsgrads von bis zu 5 % ohne Verwendung von auf dem Boden erfassten Referenzdaten. Für ATCOR-4 war die Genauigkeit Reflexionsgrads mit radiometrischen Selbstkalibrierung des Sensors besser als 5 %. Diese Ergebnisse zeigen, dass eine effiziente radiometrische Korrektur von multispektralen Luftbildern in einer photogrammetrischen Produktionsumgebung möglich ist.

## 1 Introduction

Multispectral digital aerial images are collected and used in huge amounts daily around the world. They are geometrically referenced, but the colour manipulations are relative, user dependent, and often local. Even if the images are used in automatic classification and interpretation tasks, the

methods and results are valid only for the images used. If the images can be converted to spectral reflectance, which is a non-ambiguous surface property, the automatic use of images would become easier. In this study, the objective of the radiometric correction is the reflectance image generation.

Converting the digital number (DN) of a pixel to a surface reflectance using atmospheric models is well known and standard procedure with satellite images (RICHTER 1990, CHAVEZ 1996). Such methods have also been established for airborne imaging spectroscopy (RICHTER 1996). However, radiometric correction methods are rare with aerial photogrammetric images. Wider field of view of sensors, smaller ground sampling distance (GSD), large number of images and significant BRDF (bidirectional reflectance distribution function) -effects makes the radiometric correction of aerial images more demanding compared to satellite and small FOV imaging spectroscopy images. In recent years, radiometric calibration and correction has been investigated for several photogrammetric sensors (BEISL et al. 2008, MARKELIN et al. 2008, RYAN & PAGNUTTI 2009, MARTINEZ et al. 2010). A method called radiometric aerotriangulation has been proposed for relative and absolute radiometric correction of the frame image mosaics (CHANDELIER & MARTINOTY 2009, COLLINGS et al. 2011).

In May 2008, EuroSDR (European Spatial Data Research) launched a project called "Radiometric aspects of digital photogrammetric images" to investigate the issues of accurate radiometric processing in the photogrammetric image production line. The first phase of the project consisted of a literature review and a questionnaire (HONKAVAARA et al. 2009). The major conclusions of the questionnaire were that improvements were desired for the entire process: sensors, calibration, data collection, data post-processing and data utilization. The basic radiometric end products requested by image users were true colour images and reflectance images. The expected benefits of a more accurate radiometric processing included a more automatic and efficient image post-processing, better visual image quality, more accurate and automatic interpretation, and quantitative use of image data. Based on the results of the questionnaire, an empirical phase was launched to study the following topics: 1) radiometric calibration and characterization, 2) spatial resolution assessment, 3) radiometric correction and image block equalization, 4) colour enhancement of the calibrated data 5) application oriented studies. This article studies the topics 1 and 3.

The objective of this paper is to present the main results of the performance evaluation of the radiometric correction methods for ADS40 imagery collected on 23rd of August 2008 in Hyytiälä, Finland. This evaluation was carried out in the context of the EuroSDR project. The data was processed using two commercially available processing lines: the XPro software of Leica Geosystems and the ATCOR-4 software of ReSe Applications Schläpfer. Three participants carried out the processing as follows: Swisstopo (ST) (XPro), ReSe Applications Schläpfer (ATCOR-4) and Finnish Geodetic Institute (FGI) (XPro and ATCOR-4). The same dataset is used also for tree species classification in KORPELA et al. (2011) and HEIKKINEN et al. (2011). The evaluated image versions present different scenarios for performing flight campaigns aimed for producing reflectance images: with or without accurate in-situ measurements of atmospheric parameters and with or without a possibility for vicarious in-flight radiometric calibration of the sensor.

Comprehensive results of all participants and detailed description of evaluated methods will be published in the final report of the EuroSDR-project. This study is a continuation of the first results presented in MARKELIN et al. (2010) and HONKAVAARA et al. (2011).

The article is arranged as follows: in Section 2, theories of the radiometric correction methods are briefly described. Sections 3 and 4 present the materials and methods used. Section 5 presents the main results, results are discussed in Section 6 and, finally, conclusions are given in Section 7.

## 2 Radiometric correction theory

### *2.1 Radiative transfer theory*

In a simplified case, the key formula to radiometric correction is the model for surface reflectance:

$$\rho = \frac{\pi\left((c_0 + c_1 DN) - L_0\right)}{T_{down} T_{up} S \cos\theta_i} \tag{1}$$

where ϱ is the surface reflectance, $c_0$ and $c_1$ are sensor calibration parameters, DN is target recorded digital number, $L_0$ is the path radiance, $T_{down}$ is the total downward transmittance from the top of the atmosphere (TOA) to the ground, $T_{up}$ is total upward transmittance from ground to sensor, S is the mean extraterrestial solar irradiance and $\theta_i$ is the solar zenith angle. (BEISL etl al. 2008, RICHTER & SCHLÄPFER 2011)

BEISL et al. (2008) give the following model for the sensitivity of the surface reflectance model (eq. 1): if the multiple reflection is not taken into consideration, the error in surface reflectance $\Delta\varrho$ caused by the path radiance uncertainty $\Delta L_0$ is:

$$\Delta\rho = \frac{\partial\rho}{\partial L_0}\Delta L_0 \approx -\frac{\pi}{T_{down}T_{up}S\cos\theta_i}\Delta L_0 \qquad (2)$$

Based on the (eq. 1) and (eq. 2), a number of important conclusions can now be drawn. First, an accurate radiometric calibration of the sensor is required. Secondly, an accurate estimate of the main atmospheric parameters (aerosol type, visibility or optical thickness, water vapor) is necessary, because these influence the values of path radiance, transmittance and global flux. Also, if the main atmospheric parameters and the reflectance of two reference targets are known, the quantities $L_0$, $T_{up}$, $T_{down}$, S and ϱ are known. So, a vicarious in-flight radiometric calibration of the sensor can be performed (RICHTER & SCHLÄPFER 2011). In order to keep the output reflectance error small, the path radiance error $\Delta L_0$ has to be kept as small as possible. Especially the dark surfaces of low reflectance are sensitive in this respect. Eq. (2) also shows that the absolute reflectance error becomes larger for smaller transmission, i.e. for a hazy atmosphere.

### *2.2 Leica XPro*

Leica XPro is a photogrammetric software used for the entire post-processing workflow of the ADS-imagery from data download to the generation of stereo models and orthoimages. The default product of the XPro is calibrated DN, which relates the pixel data to at-sensor radiances (ASR). In radiometric terms, the main feature of the XPro is the option to produce radiometrically corrected reflectance images. This option for atmospheric correction for reflectance image production is based on the physical modelling of radiative transfer equations and parametrization of the atmospheric parameters. To speed up the calculations, some simplifications are done in the physical modelling and parametrization of the atmosphere. In surface reflectances, the reflected radiance is divided by the incoming solar irradiance which results in a surface property. Additionally, BRDF correction based on a modified Walthall model is implemented in XPro. All corrections in XPro rely entirely on a priori sensor calibration information and atmospheric information derived from dark pixels (and bright pixel statistics for BRDF-correction) in the image data. The atmospheric correction algorithm of XPro is based on the radiative transfer equation by KAUFMAN & SENDRA (1988). Eq. (2) shows, that the accurate radiometric correction in XPro requires a careful selection of the dark pixels. The details of the XPro radiometric correction methods are given in BEISL et al. (2008) and the method and its limitations are further studied in HEIKKINEN et al. (2011).

### *2.2 ATCOR-4*

The second radiometric correction method evaluated within this paper is based on the technology of the ATCOR-4 atmospheric compensation procedure (RICHTER & SCHLÄPFER 2011). This program is one of the established standards for atmospheric compensation of optical and thermal airborne remote sensing imagery. It follows a physical approach by inverting the MODTRAN® radiative transfer code and includes the correction for terrain influences, adjacency effects, spatial water vapor distribution, aerosol content variations and variation of direct and diffuse illumination. The software uses a precompiled look-up-table (LUT) for this inversion. This LUT has been resampled to the ADS spectral response using the standard description of the spectral bands. The aerosol distribution has

been either derived by the dark dense vegetation approach (DDV) or by a generic constant (which mostly affects the blue spectral band). The output in the optical domain is the surface reflectance cube and in the thermal domain it is the surface (brightness) temperature and emissivity spectrum. ATCOR-4 is for wide FOV airborne scanner imagery and for all terrain types, and it includes the capability for radiometric correction in rugged terrain with cast shadow and illumination calculations. The in-flight radiometric calibration tool within ATCOR-4 allows user to feed a number of ground reference spectra using a good estimate of the atmospheric parameters from the given boundary conditions in order to find new gains and offsets for all spectral bands of an instrument.

In the optical domain (wavelength < 2.5 μm), assuming a flat terrain, and avoiding the specular and backscattering regions, an accuracy of the retrieved surface reflectance of ±0.02 ( for reflectance < 0.1) and ±0.04 reflectance units ( for reflectance > 0.4) is reported to be achievable for ATCOR-4 (RICHTER & SCHLÄPFER 2002).

## *3* Materials

### *3.1 Imagery*

A flight campaign was carried out at the Hyytiälä forestry research station in Finland on 23rd of August, 2008 using a Leica ADS40 SH52 digital photogrammetric camera to validate the sensor performance and to evaluate data performance in forestry applications. A total of 15 flight lines were collected from four flying heights (1, 2, 3 and 4 km, resulting GSDs of 10, 20, 30 and 40 cm, respectively). Reference targets were visible on 10 of these flight lines (Tab. 1). The MS channels (red (R), green (G), blue (B), NIR (N), both nadir and 16° backward directions) were recorded in raw (uncompressed) mode.

The weather conditions were mostly clear, but some small clouds occurred during the capturing of the 3 km and 4 km flight lines. The detailed information of the images used and atmospheric conditions during the campaign are shown in Tab. 1. Visibility, Temperature and $CO_2$ values are from the local SMEAR-II station and $O_3$, $H_2O$ and AOT values from the AERONET station. The aerosol measurement accuracies were not considered in this study.

**Tab. 1.** ADS40 flight description. Line = name of the Image line; F.h. = flying height; GSD = Ground Sampling Distance; F. Dir. = flying direction( north = 0); CF = configuration (N = nadir, B = 16° backward looking line); SenZen = average sensor zenith angle for tarps; IT = Integration time; Sun Alt. and Az. = sun altitude from horizon and sun azimuth angle (0 = north); Vis. = horizontal visibility (meteorological range); T = air temperature; AOT = aerosol optical thickness. All times are in UTC+3. All angles are in degrees.

| Line | F. h. [km] | GSD [cm] | F. Dir. | CF | SenZen (N / B) | IT [ms] | Start time | End time | Sun Alt. | Sun Az. | Vis. [km] | T [°C] | $CO_2$ [ppm] | $O_3$ [g/cm$^2$] | $H_2O$ [g/cm$^2$] | AOT 500nm |
|---|---|---|---|---|---|---|---|---|---|---|---|---|---|---|---|---|
| 1A | 1 | 10 | 349 | N | 14.7 | 1.94 | 9:56 | 10:00 | 27.1 | 119.2 | 47.8 | 13.6 | 379 | 6.54E-04 | 1.45 | 0.17 |
| 1B | 1 | 10 | 349 | N | 15.0 | 1.94 | 10:25 | 10:28 | 30.0 | 126.6 | 49.6 | 14.6 | 373 | 6.54E-04 | 1.41 | 0.16 |
| 1C | 1 | 10 | 169 | B | 21.4 | 1.94 | 10:33 | 10:36 | 30.8 | 128.7 | 44.4 | 14.7 | 373 | 6.54E-04 | 1.44 | 0.17 |
| 2A | 2 | 20 | 349 | N | 3.5 | 2.77 | 10:45 | 10:48 | 31.8 | 131.9 | 42.8 | 14.9 | 372 | 6.54E-04 | 1.40 | 0.15 |
| 2B | 2 | 20 | 349 | B | 16.2 | 2.77 | 11:00 | 11:03 | 33.1 | 136.0 | 48.9 | 14.8 | 374 | 6.54E-04 | 1.45 | 0.15 |
| 3A | 3 | 30 | 349 | N B | 3.3/16.0 | 4.16 | 11:18 | 11:20 | 34.5 | 141.0 | 50.0 | 15.0 | 374 | 6.54E-04 | 1.45 | 0.17 |
| 3B | 3 | 30 | 169 | N B | 28.8/32.2 | 4.16 | 11:25 | 11:28 | 35.0 | 143.0 | 47.8 | 15.5 | 374 | 6.54E-04 | 1.43 | 0.17 |
| 3C | 3 | 30 | 260 | N B | 1.1/15.7 | 4.16 | 11:33 | 11:35 | 35.6 | 145.3 | 46.8 | 15.4 | 373 | 6.54E-04 | 1.40 | 0.17 |
| 4A | 4 | 40 | 169 | N B | 10.7/18.8 | 5.54 | 11:43 | 11:47 | 36.2 | 148.3 | 50.0 | 15.5 | 372 | 6.54E-04 | 1.39 | 0.16 |
| 4B | 4 | 40 | 260 | N B | 0.2/15.6 | 5.54 | 11:52 | 11:54 | 36.8 | 150.9 | 50.0 | 15.5 | 373 | 6.54E-04 | 1.38 | 0.16 |

### *3.2 Ground reference measurements*

During the campaign, nadir spectra of the reference reflectance targets (portable tarpaulins, called tarps) and several other targets (asphalt road, gravel road, beach volley field sand, football field grass) were measured using an ASD Field Spec Pro FR spectroradiometer (Tab. 2, Fig. 1). Each target was measured 10-20 times on different places, and these measurements were averaged to get the final nadir field reference spectra ($\varrho_{field\_nadir}$). The tarps are flat, well defined targets whose colours are made

as lambertian as possible. The other targets used present typical flat homogenous targets that can be found on an average campaign area.

**Tab. 2.** Ground reference targets. SH = short name for target; n = number of spectra measured; Time = measurement time (UTC+3); Sun Alt. and Az. = sun altitude from horizon and sun azimuth angle (0 = north); Refl. = average target reflectance on green channel (550 nm); CV% = ground measurement Coefficient of Variation (100*stdev/mean) for green channel.

| SH | Target | n | Time | Sun Alt. | Sun Az. | Refl. | CV% |
|---|---|---|---|---|---|---|---|
| A | asphalt | 13 | 9:59 | 27.4 | 120.0 | 0.140 | 2.8 |
| B | grass1 | 15 | 10:08 | 28.4 | 122.2 | 0.078 | 4.9 |
| C | grass2 | 10 | 10:16 | 29.1 | 124.3 | 0.068 | 9.6 |
| E | sand | 20 | 10:44 | 31.7 | 131.6 | 0.187 | 21.0 |
| F | gray gravel1 | 14 | 10:54 | 32.6 | 134.4 | 0.090 | 8.7 |
| G | gray gravel2 | 14 | 11:00 | 33.1 | 136.0 | 0.090 | 8.3 |
| P05 | tarpaulin 05 | 15 | 10:21 | 29.6 | 125.6 | 0.057 | 4.9 |
| P20 | tarpaulin 20 | 15 | 10:25 | 30.0 | 126.6 | 0.181 | 2.8 |
| P30 | tarpaulin 30 | 12 | 10:29 | 30.4 | 127.7 | 0.261 | 5.6 |
| P50 | tarpaulin 50 | 20 | 10:33 | 30.8 | 128.7 | 0.442 | 2.9 |

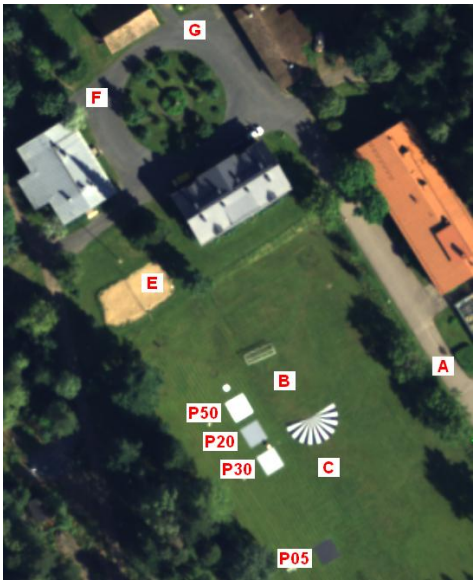


**Fig. 1.** Reference targets in field. For abbreviations, see Tab. 2.

## 4 Methods

### *4.1 General*

A total of 12 different reflectance image products were created using the XPro and ATCOR-4 software systems. Options for sensor radiometric calibration were laboratory calibration by the sensor manufacturer and vicarious in-flight calibration performed during the data processing. Atmospheric correction parameters were either based on in-situ measurements or estimated from the images. Tab. 3 shows all the different processing versions evaluated in this article. All image lines (Tab. 1) were processed with XPro, resulting in versions XA1 and XF1 by FGI. FGI also processed four nadir looking image lines (1B, 2A, 3A and 4A) with ATCOR-4, resulting in versions AL1, AL2, AV1, AV2 and AV3. Swisstopo processed the nadir looking lines 2A, 4A and 4B with XPro (versions XA2 and XF2), and ReSe processed the nadir looking line 2A with ATCOR-4, referred to as versions AL3, AV4 and AV5.

All image versions obtained by XPro and the ATCOR-4 versions AL2 and AL3 present a typical flight campaign with a laboratory-calibrated sensor, when no ground reference measurements or in-situ atmospheric observations exist. Version AL1 is the same but with detailed in-situ atmospheric observations. The ATCOR-4 processed versions AV2, AV4 and AV5 are examples of the situation when vicarious calibration of the sensor can be performed with ground reference targets, but there is no accurate information of atmospheric parameters. AV1 presents the case when extensive in-situ reference measurements provide a possibility to vicarious calibration of the sensor and atmospheric correction with in-situ atmospheric data. Finally, the ATCOR-4 processed version AV3 presents the situation where detailed vicarious calibration of the sensor is performed using a number of four reference spectra in one image line and then the same sensor calibration is used in the processing of the rest of the images.

**Tab. 3.** Processing parameters of all evaluated image versions (X for XPro, A for ATCOR-4).; Cal.: origin of the sensor radiometric calibration (lab: laboratory, vic: vicarious in-flight radiometric calibration with tarps P05 and P50); Atm.: origin of the atmospheric parameters used (imag: derived from the imagery, in-situ: in-situ measurements). Other: BRDF = with empirical BRDF-correction, cal.1B = sensor calibration based on image line 1B and all four tarps; shd. = with shadow removal.

| | XA1 | XA2 | XF1 | XF2 | AL1 | AL2 | AL3 | AV1 | AV2 | AV3 | AV4 | AV5 |
|---|---|---|---|---|---|---|---|---|---|---|---|---|
| Participant | FGI | ST | FGI | ST | FGI | FGI | ReSe | FGI | FGI | FGI | ReSe | ReSe |
| Cal. | lab | lab | lab | lab | lab | lab | lab | vic. | vic. | vic. | vic. | vic. |
| Atm. | imag. | imag. | imag. | imag. | in-situ | imag. | imag. | in-situ | imag. | imag. | imag. | imag. |
| Other | | | BRDF | BRDF | | | | | | cal.1B | | shd. |

### *4.2 XPro processing*

FGI used the Leica XPro version 4.1 for the entire post-processing workflow of the ADS-imagery from data download to the generation of stereo models and orthoimages (versions L2). The later version 4.2 of XPro was used for BRDF-corrections. Geometric processing was done using 12 ground control points (GCPs) and 47 check points. The RMS residuals (in m) for check points after triangulation were the following: x:0.067 , y: 0.050, z: 0.090 (1 km flying height); x: 0.050, y: 0.044, z: 0.113 (2 km); x: 0.058, y:0.061 , z: 0.105 (3 km); x: 0.062, y: 0.078, z: 0.171 (4 km). These results indicate excellent geometric accuracy.

In radiometric processing, all images were processed without any atmospheric corrections to at-sensor radiance data. The accuracy of the XPro ASR-product was studied in MARKELIN et al. (2010). Next, both FGI and Swisstopo processed radiometrically corrected surface reflectance images (Tab. 3 XA1-2) and radiometrically corrected versions with BRDF-correction (Tab. 3 XF1-2), i.e. surface reflectance data corrected to nadir looking geometry. FGI used the XPro version 4.2 for BRDF-correction because it included an updated water masking algorithm compared to the previous version. The default settings of XPro were used for the BRDF-correction.

Swisstopo used the Leica XPro version 4.2 for the data processing. Since their aim was to test the software and not the know-how of the user, Swisstopo decided to keep the default settings given by Leica Geosystems for the statistics generation and all applied corrections.

### *4.3 ATCOR-4 processing*

The starting point for the ATCOR-4 processing was the nadir looking L2 orthorectified ASR-versions of the ADS-imagery created with XPro. For the processing, standard values for the water vapor amount has been taken into account as this parameter is of minor influence in the ADS spectral wavelength range.

ReSe used the following processing steps with ATCOR-4. First, the solar and flying geometries were defined for each image. Then ATCOR-4 was started with the gain values provided in the sensor specific Leica calibration files, and the derived surface reflectance outputs were visually checked

(Tab. 3 AL3). Next the in-field targets were used to perform an in-flight vicarious calibration, which lead to updated gain/offset values. The atmospheric correction was repeated using the in-flight calibration coefficients (Tab. 3 AV4). Finally the cast-shadow correction and building/tree correction was tested and applied on the basis of in-flight calibrated data (Tab. 3 AV5).

The FGI processing was done using the ATCOR-4 software version 5.1. Small subsets of the size about 2 km x 2 km were cropped from the original image lines. Because of limitations with the available system memory, images from flying heights 1, 2 and 4 km were resampled to 40 cm GSD and the image from the 3 km flying height to 60 cm GSD. Five different radiometrically corrected versions were then calculated for each flying height (Tab. 3 and Tab. 4). In versions AL1 and AL2, the sensor radiometric calibration parameters were taken from Leica Geosystems (i.e. how the DNs of ASR-images were converted to at-sensor radiances). In versions AV1 and AV2 the sensor calibration parameters were determined individually for each image by using the ATCOR-4 in-flight calibration module and spectra of reference reflectance targets P05 and P50. In AV3, the sensor calibration parameters were determined from the 1 km flying height image 1B and using in-flight calibration with all the four reference reflectance targets. Atmospheric parameters (aerosol type, water vapor and visibility) for the versions AL1 and AV1 were set based on the in-situ atmospheric measurements (Tab. 3). For the versions AL2, AV1 and AV3 the atmospheric parameters were derived from the image data using the ATCOR-4 modules; also the variable visibility option was activated. Tab. 4 shows the final atmospheric parameters used in the ATCOR-4 processing (compare to in-situ measurements in Tab. 1).

The influence of topography was not considered in the ATCOR-4 processings as the test area is mostly flat.

**Tab. 4.** Atmospheric parameters used in ATCOR-4 processing for flight lines 1B, 2A, 3A and 4A. aer: aerosol type (rural, urban, maritime or desert), vis: horizontal visibility in km, AOT: aerosol optical thickness at 550 nm

| | 1B | | | 2A | | | 3A | | | 4A | | |
|---|---|---|---|---|---|---|---|---|---|---|---|---|
| | aer. | vis. | AOT | aer. | vis. | AOT | aer. | vis. | AOT | aer. | vis. | AOT |
| AL1, AV1 | rural | 49.6 | 0.165 | rural | 42.8 | 0.187 | rural | 50 | 0.164 | rural | 50.0 | 0.164 |
| AL2 | rural | 83.1 | 0.108 | mari. | 88.9 | 0.098 | mari. | 95.4 | 0.095 | mari. | 95.4 | 0.094 |
| AV2 | rural | 62.3 | 0.137 | rural | 69.4 | 0.125 | rural | 73.4 | 0.119 | rural | 73.4 | 0.123 |
| AV3 | rural | 62.3 | 0.137 | rural | 73.4 | 0.123 | rural | 78 | 0.113 | rural | 83.1 | 0.103 |
| AL3, AV4, AV5 | | | | urban | 80.0 | 0.110 | | | | | | |

## *4.4 Analysis methods*

Reflectance of all ground reference targets (Tab. 2) were measured from the images; the size of the measurement window was 3 m x 3 m in object coordinates. These measurements provided the target data reflectance ($\varrho_{data}$). The exact measurement places of targets other than tarps were ambiguous (measurement place between image lines, and difference between field reference measurement and image measurement), especially on grass, which may add some uncertainty to the results.

As a reference reflectance, laboratory measurements with the FIGIFIGO goniospectrometer (SUOMALAINEN et al. 2009) in the exact imaging geometry, scaled with the nadir field measurements were used. This scaling was done to match the laboratory measurements to the actual imaging conditions. The reference reflectance for tarps is:

$$\rho_{ref} = \rho_{lab\_exact} \frac{\rho_{field\_nadir}}{\rho_{lab\_nadir}} \tag{3}$$

where $\varrho_{field\_nadir}$ is the target nadir reflectance measurement during the imaging campaign, $\varrho_{lab\_nadir}$ is the target nadir reflectance measured at the laboratory, and $\varrho_{lab\_exact}$ is the target reflectance at the exact imaging geometry (illumination and viewing angles) of the respective image.

The difference of the target image reflectance and the reference reflectance was calculated to obtain the reflectance error in reflectance units:

$$E_{refl} = \rho_{data} - \rho_{ref} \tag{4}$$

Next this difference was divided by the reference and multiplied by 100 to get the reflectance error in percents:

$$E_{refl\%} = 100\ (\rho_{data} - \rho_{ref})/\rho_{ref} \tag{5}$$

The $E_{refl}$ and $E_{refl\%}$ were calculated for all tarps, images, and colour channels. From these errors, root mean square error values ($RMSE_{refl}$ and $RMSE_{refl\%}$) were calculated using all of the four tarps (except when the targets were used in the sensor calibration) for each image line and channel. The $RMSE_{refl\%}$ is:

$$RMSE_{refl\%} = \sqrt{\frac{\sum E_{refl\%}^2}{n}} \tag{6}$$

where *n* is the number of targets used.

For a relative comparison of the different flying heights, 2 km, 3 km and 4 km data were compared to 1 km data, which was used as reference. For tarps, the data was first scaled to nadir view using laboratory calculated anisotropy factors:

$$\rho_{data\_nadir} = \rho_{data}\frac{\rho_{lab\_nadir}}{\rho_{lab\_exact}} \tag{7}$$

Next, relative differences were calculated between 1 km reference data and 2 km, 3 km and 4 km data using eq. 5, and finally $RMSE_{refl\%}$ was calculated using eq. 6.

For targets other than tarps (asphalt, sand, gravel, grass) the same kind of calculations for $E_{refl}$ and $E_{refl\%}$, $RMSE_{refl}$, $RMSE_{refl\%}$ and relative flying height comparison were carried out, but nadir field measurements were used as reference. This means that the anisotropy effects of targets on images with large viewing angles are included in the results, which can add some error. The grass was processed separately from the other non-organic targets.

The reflectance error is given in most cases as percents of magnitude of the reflectance; we specify the cases separately where the error is given in reflectance units.

The dependency of $E_{refl}$ and $E_{refl\%}$ on the magnitude of reflectance was evaluated by plotting these errors against the reference reflectance. Linear fit parameters (gain, offset and $R^2$-value) were calculated for the data and the dependency was analyzed based on the $R^2$-values.

## 5 Results

The main results of the study are presented in the following sub sections. The most thorough analysis is shown for the tarps, because they had the most accurate reference and tarps are unambiguous as targets. Only selected results are shown for other targets. Comprehensive results of all participants and all processing methods will be published in the final report of the EuroSDR project.

### *5.1 General results*

First we made some some general evaluations of the data to remove identical results.

A. The reflectance accuracy was evaluated both in reflectance error in reflectance units (eq. 4) and reflectance error in percents (eq. 5). Both methods lead to the same conclusions, so only results with reflectance error in percents (and $RMSE_{refl\%}$) are shown.

B. The results with the dark tarp (P05) are presented separately from the bright tarps (P20, P30 and P50), because the reflectance of dark target is sensitive to errors in path radiance modelling. Also the detection accuracy of dark pixels is essential in the evaluated XPro methods and a small inaccuracy will cause a large relative error in dark areas.

C. The XPro processing results of Swisstopo and FGI were practically the same, so only the FGI results are shown in most cases.

D. The XPro correction versions XA and XF provided a mostly similar accuracy. Because the Hyytiälä area is mostly forest and the XPro BRDF-correction is based on DN averages over large areas, the BRDF-correction is not expected to work accurately enough with tarps. So results with the XF-versions are considered only with the grass target.

E. The XPro results for nadir and 16° backward looking lines were mostly similar (especially when both views were collected simultaneously, i.e. for the 3 and 4 km flying heights), so in most cases only nadir results are shown.

F. For the cases where similar results were obtained on different passes, averages per flying height were calculated for XPro with tarps.

G. The ATCOR-4 processing results with atmospheric parameters set by the user (AL1 and AV1) and parameters derived automatically from the images (AL2 and AV2) provided similar results, so only results with AL2 and AV2 are shown.

The reflectance error (eq. 4) was dependent on the magnitude of the reflectance, which could be compensated to a large extent by evaluating reflectance errors in percents (eq. 5).

Some small clouds moved over the test area during the capturing of the 3 km and 4 km flying height lines. By visual inspection, these clouds or their shadows did not overshadow the reference targets, but it is possible that the clouds had some effect on the results.

The shadow removal method used in the ATCOR-4 processing version AV5 erroneosly interpreted many dark objects (e.g. tarp P05) as shadows (Fig. 3 top).

The results with tarps for ATCOR-4 processings version AV3 are not independent, because the same tarps were also used with the sensor calibration. These results are still shown for comparison. The accuracy of the method AV3 (as well as all the methods) is evaluated also with other (independent) targets.

Fig. 2 shows an example of the reflectance spectra of the reference targets derived from the imagery.

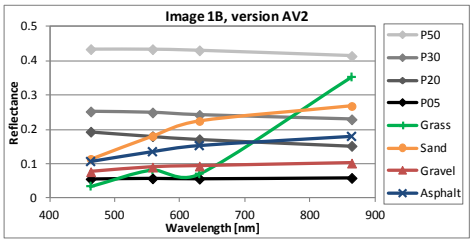


**Fig. 2.** Reference target reflectance spectra for image 1B (1 km flying height) with AV2 processing. Marks show ADS40 channels.

### *5.2 Reflectance accuracy with tarps*

A reflectance accuracy better than 5 % was achievable with all the evaluated methods. Results varied depending on the target, colour channel, origin of the sensor radiometric calibration, flying height and

weather conditions. Fig. 3 shows the reflectance error for the dark tarp and $RMSE_{refl\%}$ for the bright tarps for the XPro and ATCOR-4 nadir looking lines. In Fig. 4, $RMSE_{refl\%}$ of all lines processed with XPro are shown.

The reflectance error was on average higher for the dark tarp (often over 10 %, Fig. 3 top) than for the bright tarps (mostly below 10 %, Fig. 3 bottom). On the other hand, the reflectance error in reflectance units was smaller (below 0.01) for the dark tarp than for the bright tarps (below 0.04). This behaviour was expected, because even small reflectance errors for a dark object become large when scaled to %.

On the bright tarps, the green, red and sometimes NIR-channel provided the best results and the blue channel the worst (Fig. 3 bottom). The green and red channels behaved similarly compared to each other. The NIR channel was the worst on the 2 km flying height on ATCOR-4 methods AL2, AL3, AV4 and AV5. On the dark tarp, the NIR channel gave the worst results for the 3 and 4 km flying heights (Fig. 3 top).

The vicarious calibration of the sensor improved the results with ATCOR-4 on all methods, except for the NIR channel with the dark tarp (Fig. 3).

The effect of flying height was minor with XPro except for the blue channel, on which the reflectance accuracy was clearly worse for the 3 and 4 km flying heights compared to the 1 and 2 km flying heights (Fig. 4). With ATCOR-4, the reflectance errors from the 3 and 4 km flying heights were slightly higher (over 5 %) than for the 1 and 2 km flying heights (below 5 %) (Fig. 3).

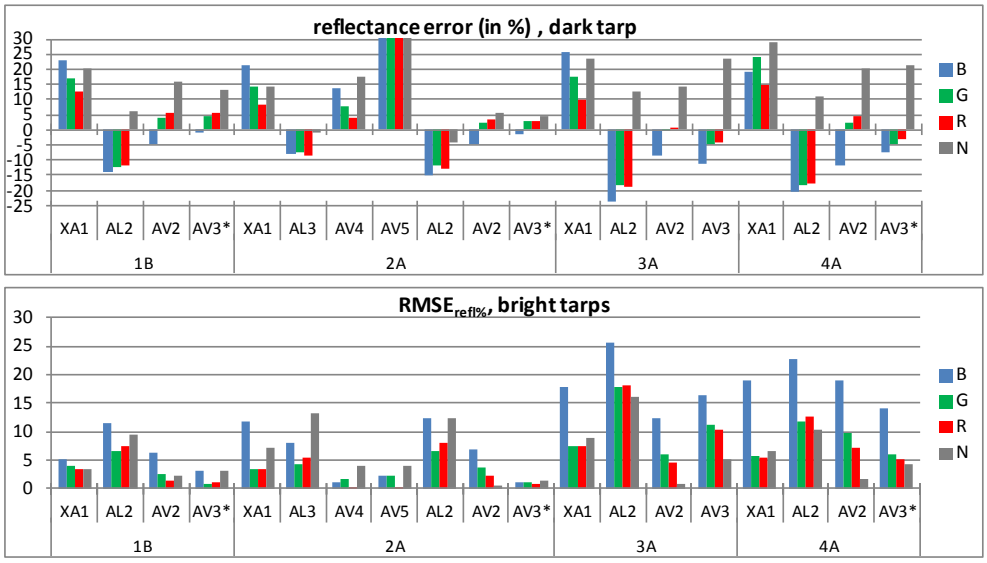


**Fig. 3.** Reflectance error (in %) for the dark tarp (top) and $RMSE_{refl\%}$ for the bright tarps (bottom). The values for XPro are averages of all image lines for a certain flying height. * denotes that the results for AV3 are not independent. For AV5 dark tarp image 2A, the reflectance error values are B: 62%, G: 81%, R: 79% and NIR: 121%.

With the XPro there appeared a clear dependency of the reflectance error to the magnitude of reflectance - both in reflectance units and in percents (modelled as linear in this investigation). As an example, in Fig. 5 reflectance errors in reflectance units and in percents are shown as a function of the reflectance for the XPro XA1 versions of lines 4A and 4B. Fig. 5 includes tarpaulins with exact reference and non-organic targets with nadir field reference. The dependency of reflectance errors (in reflectance units) to magnitude of reflectance was clear for all XPro and ATCOR-4 methods and all colour channels with flying heights 3 km and 4 km. For XPro, this dependency was detected also for

the red and green channels with the 2 km flying height and the blue-channel with the 1 km flying height imagery. After scaling to reflectance errors (in %), the $R^2$ values for linear fit lowered clearly with all ATCOR-4 methods, except for the blue and green channels for the 2 km flying height and the NIR-channel for the 3 and 4 km flying heights with the methods including sensor laboratory calibration (AL1-AL3). For XPro, the dependency of reflectance error to magnitude of reflectance remained after the scaling of reflectance errors to percents.

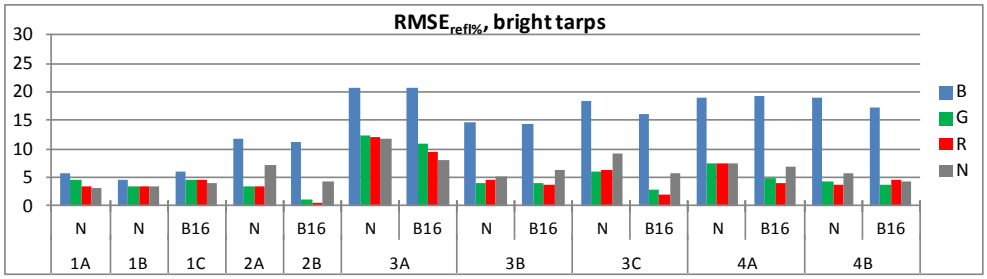


**Fig. 4.** $RMSE_{refl\%}$ for XPro, bright tarps, all lines, XA1 versions. N = nadir looking, B16 = backward looking image line.

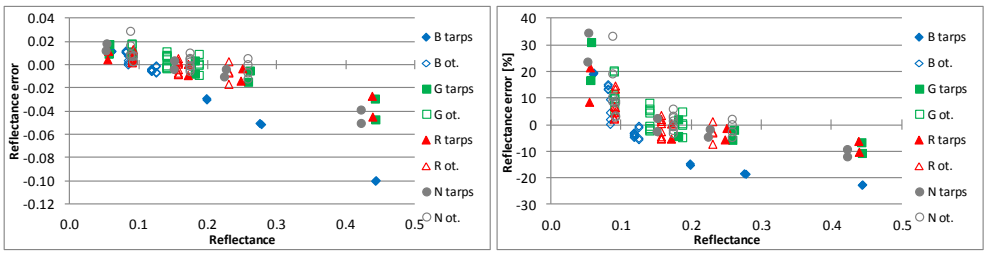


**Fig. 5**. Reflectance error for the XPro XA1 versions of nadir looking lines 4A and 4B. Reflectance error in reflectance units (left) and reflectance error in percent (right). Filled marks are for tarps, open marks for non-organic targets (asphalt, gravel, sand).

### *5.3 Reflectance accuracy with other targets*

The $RMSE_{refl\%}$ results for non-organic (asphalt, gravel, sand) and grass targets are shown in Fig. 6. Both XPro and ATCOR-4 provided reflectance accuracy better than 5 % at best. For non-organic targets, XPro and ATCOR-4 with vicarious calibration of the sensor (AV1 - AV5) produced stable $RMSE_{refl\%}$ between 5 and 10 % on all flying heights with some exceptions. ATCOR-4 with sensor laboratory calibration (AL1 – AL3) provided a slightly higher reflectance error (5 to 20 %) compared to versions with vicarious calibration of the sensor (AV1 – AV5) (Fig. 6 top).

The grass targets provided variable results on all methods, both in errors in reflectance units and in percents. In reflectance errors in reflectance units the NIR-channel gave the worst results, between 0.04 to 0.13. On the other channels, the errors were mostly below 0.02. In $RMSE_{refl\%}$ the XPro blue channel gave the worst results, 40 % and more; the green and red channels gave a $RMSE_{refl\%}$ below 25 % and the NIR-channel below 20 %, sometimes even below 10 %. On the ATCOR-4 methods, the blue and green channels provided the lowest errors, sometimes even below 5 %. $RMSE_{refl\%}$ on the red and NIR-channels were mostly between 10 and 20 %. For blue and green channel, methods AL2, AV2 and AV3 provided sometimes even better $RMSE_{refl\%}$ results with grass targets than with tarps or other targets. The empirical XPro BRDF-correction on the FULL-versions (XF1) did not provide significant improvement compared to the radiometric correction (XA1) only (Fig. 6 bottom).

The reflectance accuracy on different objects can be compared based on the Fig.s 3 (bottom), 6 (top) and 6 (bottom). The results with tarps and non-organic targets were quite similar: on low flying

altitudes (1 and 2 km) tarps were mostly better; for higher altitudes the results were similar on green and red channels, tarps provided better results on NIR-channel and other targets on blue channel. Variability of results was clearly higher with the grass target, which is caused mostly by the vagueness of the object.

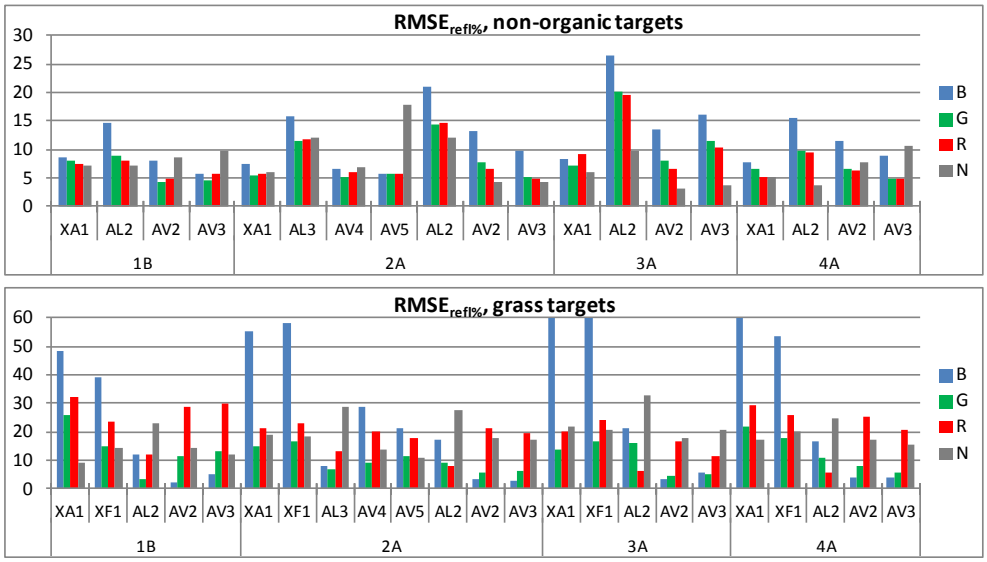


**Fig. 6.** $RMSE_{refl\%}$ results for non-organic (top; asphalt, gravel and sand) and grass targets (bottom). The $RMSE_{refl\%}$ values for grass targets, blue channel, image 3A method XA1 is 66%, XF1 71% and image 4A method XA1 61%.

### *5.4 Comparison of methods*

The $RMSE_{refl\%}$ results for the bright tarps of all processing methods evaluated for the 2 km flight line 2A are shown in Fig. 7. All but the AL2 could produce a $RMSE_{refl\%}$ below 5 % at least on some channels. For XPro, the green and red channels provided the best results and the blue the worst. For the ATCOR-4 versions, the methods with vicarious calibration of the sensor (AV1-AV5) outperformed methods with sensor laboratory calibration (AL1-AL3).

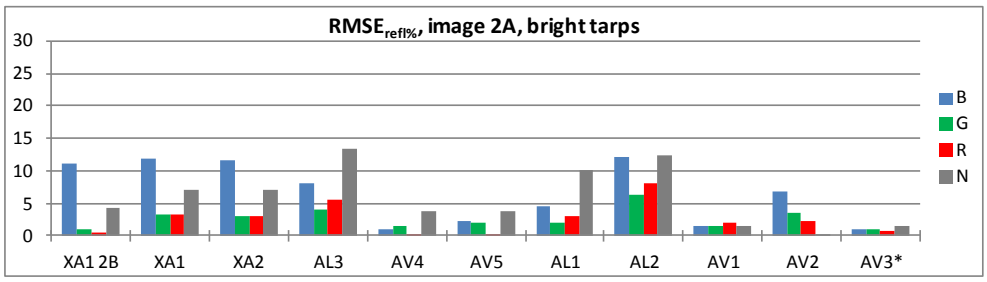


**Fig. 7.** $RMSE_{refl\%}$ results for the bright tarps (all methods, image line 2A for nadir, 2B for XA1 backward looking line) (dark tarp behaved similarly to fig. 3). * denotes that the results for AV3 are not independent.

The internal repeatibility of results with different processing methods was evaluated by comparing the

results from the 2, 3 and 4 km flying heights to 1 km flying height (Fig. 8). Both XPro and ATCOR-4 provided a difference of 5 % or less for the 2 km flying height. The difference for the 3 and 4 km flying height varied between 5 to 15 % for the blue, green and red channels, and between 2 to 10 % for the NIR-channel.

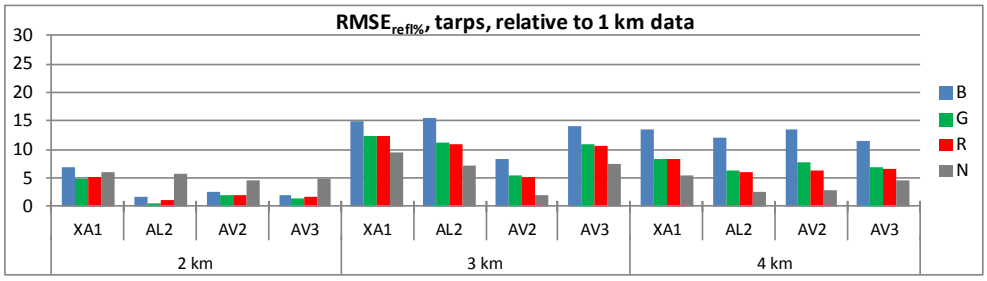


**Fig. 8.** Internal repeatibility of methods, $RMSE_{refl\%}$ comparison relative to 1 km data.

## 6 Discussion

The main focus in this article was to evaluate accuracies of reflectance images produced from the images of multispectral aerial line scanner data. In total, 12 different approaches and corrected image versions were compared. The evaluated methods included two different software systems (photogrammetric software Leica XPro and ATCOR-4 software dedicated to atmospheric correction) and the radiometrically corrected images represented both typical photogrammetric campaign without any ground reference information and a campaign with a comprehensive reference including targets, field measurements and atmospheric observations.

Even though the campaign was flown in mainly excellent weather conditions, small clouds that occurred on the campaign area during the imaging of the 3 km and 4 km image lines may have some effect on the results.

A prerequisite for the processing accuracy was the radiometrically and spectrally calibrated stable sensor. In the case of ADS40 the quality is ensured by careful lens and filter design, using temperature stabilization and fixed aperture and by accurate calibration processing. However, the reflectance products showed variation between different flying heights. In this investigation, these were most likely due to the inaccurate atmospheric and BRDF modeling, but also the sensor instability is one possible reason. Uniformity of reflectance product over the entire block area could be improved by using radiometric block adjustment methods; one approach was developed by CHANDELIER & MARTINOTY (2009) and another by COLLINGS et al. (2011).

Both evaluated software systems provided good results without accurate in-situ measured atmospheric parameters, i.e. both methods were able to estimate the needed parameters automatically from the image data itself. It may also help that Leica ADS40 is a multispectral sensor with wide spectral bands (compared to hyperspectral sensors), so the system is not so sensitive to small changes in aerosol and molecule concentrations. XPro produced stable results on all channels and flying heights with the laboratory calibration of the sensor. With ATCOR-4, the vicarious radiometric in-flight calibration of the sensor improved the reflectance accuracies of all processed images compared to the image versions with the sensor laboratory calibration. Further studies are needed to find out if this was due to sensor instability or some other reasons.

An important issue in interpretation applications is the natural variation of objects. The accuracies of the methods were tested using well-defined, flat, nearly-lambertian reference reflectance targets and typical permanent flat targets (asphalt, gravel road, sand, grass) that can be found from the coverage of the images. In our results, the reflectance errors of grass were 1 to 60 times, and on average 4.7 times higher than the reflectance errors of uniform asphalt and sand targets or tarps. The same ADS40 reflectance data sets were recently used by KORPELA et al. (2011) in forestry appliciations and in tree species classification. Evaluations showed that the variation coefficients of tree species in forests

were 13-31 % of reflectance values. High variability will decrease the separability of tree species in classification (KORPELA et al. 2011, HEIKKINEN et al. 2011).

An important advantage of the XPro reflectance image production was its efficient workflow with minimal user interaction. Also the XPro is able to process large amounts of images automatically, an essential requirement for a practical workflow, which was proven in operational conditions by Swisstopo. On the other hand, the effect of the few adjustable statistical parameters in the BRDF-correction would require further studies. For a broadband multispectral sensor like the ADS a rather simple approach of XPro for atmospheric correction gave results comparable to ATCOR-4. However, if ground reference data are available the results can be improved by the use of ATCOR-4. Adding an in-flight calibration procedure to XPro could further improve the results.

Important features of the ATCOR-4 were the possibility to vicarious in-flight radiometric calibration of the sensor and advanced methods for setting and detecting atmospheric parameters from the images, which are useful in applications with high reliability requirements. Because of the sophisticated modules and options, ATCOR-4 requires an experienced operator to produce reliable and accurate results. The results show that shadow correction method used in ATCOR-4-based method AV5 is not applicable to high spatial resolution multispectral instruments as it had been developed for 5-10 m resolution hyperspectral imagery, and requires further development for multispectral photogrammetric applications.

An improvement for both evaluated softwares would be an option for radiometric block adjustement.

## 7 Conclusions

In this article, two methods and in total 12 different processing versions for correcting the airborne multispectral ADS40 at-sensor radiance images to surface reflectance images were evaluated. The results showed that reflectance accuracy level of 5 % is possible with sensor laboratory calibration and even without any reference measurements. With vicarious radiometric in-flight calibration of the sensor, reflectance accuracies even better than 5 % were accieved.

## Acknowledgements

Our sincere acknowledgements go to Leica Geosystems, Estonian Landboard and National Land Survey of Finland for their support. We are grateful for all the collegues who helped in the field work, especially Teemu Hakala and Leena Matikainen for the field work and Juha Suomalainen for the reflectance library.

## References

BEISL, U., TELAAR, J., AND SCHÖNERMARK, M. V., 2008. Atmospheric correction, reflectance calibration and BRDF correction for ADS40 image data. - The International Archives of the Photogrammetry, Remote Sensing and Spatial Information Sciences **37**, part B7.

CHANDELIER, L., MARTINOTY, G, 2009. Radiometric aerial triangulation for the equalization of digital aerial images and orthoimages. - Photogrammetric Engineering & Remote Sensing **75** (2): 193-200.

CHAVEZ, R., 1996. Image-based atmospheric corrections - revisited and improved. – Photogrammetric Engineering & Remote Sensing **62** (9): 1025-1036.

COLLINGS, S., CACETTA, P., CAMPBELL, N., WU, X. 2011. Empirical models for radiometric calibration of digital aerial frame mosaics. - IEEE Transactions on Geoscience and Remote Sensing **49** (7): 2573-2588.

HEIKKINEN, V., KORPELA, I., TOKOLA, T., HONKAVAARA, T., PARKKINEN, J., 2011. An SVM classification of tree species radiometric signatures based on the Leica ADS40 sensor. - IEEE Transactions on Geoscience and Remote Senssing, In press.

HONKAVAARA, E., ARBIOL, R., MARKELIN, L., MARTINEZ, L., CRAMER, M., BOVET, S., CHANDELIER, L., ILVES, R., KLONUS, S., MARSHALL, P., SCLÄPFER, D., TABOR, M., THOM, C., AND N. VEJE,

2009. Digital airborne photogrammetry – A new tool for quantitative remote sensing? – A state-of-the-art review on radiometric aspects of digital photogrammetric images. - Remote Sensing **1** (3): 577-605.

HONKAVAARA, E., ARBIOL, R., MARKELIN, L., MARTINEZ, L., BOVET, S., BREDIF, M., CHANDELIER, L., HEIKKINEN, V., KORPELA, I., LELEGARD, L., PÉREZ, F., SCHLÄPFER, D., TOKOLA, T., 2011. The EuroSDR project "Radiometric aspects of digital photogrammetric images" – Results of the empirical phase. - Proceedings of the ISPRS Hannover Workshop 2011, June 14-17, 2011, 8 pages.

KAUFMAN, Y.J., SENDRA, C., 1988. Algorithm for automatic atmospheric corrections to visible and near-IR satellite imagery. International Journal of Remote Sensing 9 (8): 1357–1381.

KORPELA, I., HEIKKINEN V., HONKAVAARA E., ROHRBACH F., TOKOLA T., 2011. Variation and directional anisotropy of reflectance at the crown scale – implications for tree species classification in digital aerial images. - Remote Sensing of Environment **115** (8): 2062–2074.

MARKELIN, L., HONKAVAARA, E., PELTONIEMI, J., AHOKAS, E., KUITTINEN, R., HYYPPÄ, J., SUOMALAINEN, J., KUKKO, A. 2008. Radiometric calibration and characterization of large-format digital photogrammetric sensors in a test field. Photogrammetric - Engineering and Remote Sensing **74** (12): 1487-1500.

MARKELIN, L., HONKAVAARA, E., BEISL, U. AND KORPELA, I., 2010. Validation of the radiometric processing chain of the Leica ADS40 airborne photogrammetric sensor. - International Archives of Photogrammetry, Remote Sensing and Spatial Information Sciences **38** (7A): 145-150.

MARTÍNEZ, L., ARBIOL, R. AND PÉREZ F. 2010. CASI Characterization and atmospheric correction for EuroSDR Banyoles08 dataset. - Proceedings of the EuroCOW 2010, 4 pages.

RICHTER, R., 1990. A fast atmospheric correction algorithm applied to Landsat TM images. – International Journal of Remote Sensing **11** (1): 159-166.

RICHTER, R., 1996. Atmospheric correction of DAIS hyperspectral image data. – Computers & Geosciences **22** (7): 785-793.

RICHTER, R., SCHLÄPFER, D., 2002. Geo-atmospheric processing of airborne imaging spectrometry data. Part 2: atmospheric / topographic correction. - International Journal of Remote Sensing **23** (13): 2361 – 2649.

RICHTER, R., SCHLÄPFER, D., 2011. Atmospheric / Topographic Correction for Airborne Imagery (ATCOR-4 User Guide, Version 6.0.2, August 2011). - DLR report DLR-IB 565-02/11, Wessling, Germany, 194p. Available from http://www.rese.ch/download/

RYAN, R.E., PAGNUTTI, M., 2009. Enhanced absolute and relative radiometric calibration for digital aerial cameras. - Fritsch, D. (Ed.), Photogrammetric Week 2009. Wichmann Verlag, Heidelberg, Germany, pp. 81-90.

SUOMALAINEN, J., HAKALA, T., PELTONIEMI, J., PUTTONEN, E., 2009. Polarised multiangular reflectance measurements using the finnish geodetic institute field goniospectrometer. - Sensors **9** (5): 3891-3907.

Addresses of the Authors:

LAURI MARKELIN, EIJA HONKAVAARA, Finnish Geodetic Institute, Geodeetinrinne 2, P.O.Box 15 FI-02431 Masala Finland, Tel.: +358 9 29555239, e-mail: lauri.markelin@fgi.fi, eija.honkavaara@fgi.fi

DANIEL SCHLÄPFER, ReSe Applications Schläpfer, Langeggweg 3, CH-9500 Wil, Switzerland, e-mail: info@rese.ch

STÉPHANE BOVET, Swisstopo – Federal Office of Topography, Seftigenstrasse 264, CH 3084 Wabern, Switzerland, e-mail: stephane.bovet@swisstopo.ch

ILKKA KORPELA, University of Helsinki, Department of Forest Sciences, P.O.Box 27 FI-00014 Finland, e-mail: ilkka.korpela@helsinki